Supporting Information

Toward Record High Zn²⁺ Storage in Carbon Electrode via Pore Confinement Engineering

Xiubo Zhang, Chang Yu,[*] Yuanyang Xie, Jinhe Yu, Yingbin Liu, Yi Yang, Jianjian Wang, Shuqin Lan, Siyi Hou, Kunlun Liu, Jieshan Qiu[*]

State Key Laboratory of Fine Chemicals, Frontier Science Center for Smart Materials, School of Chemical Engineering, Dalian University of Technology, Dalian 116024, China

[*] Corresponding authors: C. Y. (Email: chang.yu@dlut.edu.cn) and J.S.Q. (Email: jqiu@dlut.edu.cn)

Experimental Section

Synthesis of BPC-x: All reagents were of analytical grade and not further purified. The BPC-x samples were prepared by pyrolysis. The sweet potato leaves as the biomass precursor were cleaned with deionized water 6 times to remove the impurities, dried to a constant weight, and crushed into a powder using a pulverizer. The precursor powder (1 g), KOH (3 g) and distilled water (5 ml) were mixed and the resulting dried solid was homogeneously ground for a duration of 10 minutes. Subsequently, the obtained mixture was kept in Ar atmosphere at 800 °C for 2 h with a heating rate of 5 °C min^{-1}. The black product obtained after carbonization was washed with deionized water 3 times at 80 °C. The black product obtained after carbonization were immersed in 80 °C of diluted HCl solution to remove impurities. Finally, the BPC-3 sample was thoroughly washed with distilled water and dried at 80 °C. In addition, the samples for comparison were also prepared using different mass ratios of precursor powder to KOH (1:0.33, 1:1, 1:2, 1:6 and 1:9) following the same process and the corresponding samples were recorded as BPC-0.33, BPC-1, BPC-2, BPC-6 and BPC-9, respectively.

Fabrication of BPC-x electrodes: Typically, with a mass ratio of 8:1:1, the BPC-x active materials, poly (tetrafluoroethylene) and acetylene black were homogeneously mixed with ethanol and dried. The obtained mixtures were rolled and punched into 10 mm (diameter) round electrodes, and dried at 80 °C. The total mass loading of carbon active material in electrode was 1.8 to 2.8 mg cm^{-2}.

Materials Characterization: Scanning electron microscopy (SEM, SU8220) and transmission electron microscopy (TEM, HT7700) were performed for morphological characterization. The chemical compositions were characterized by X-ray photoelectron spectroscopy (XPS, Thermo ESCALAB 250). The N_2 adsorption/desorption measurement was conducted using a Micromeritics ASAP 2020 analyzer. Powder XRD patterns of the samples were recorded using a Rigaku D/Max 2400 diffractometer. Raman spectrum analyses were conducted using a Thermo Fisher Scientific DXR Raman Microscope.

Electrochemical Measurements: The cyclic voltammetry (CV), galvanostatic charge/discharge (GC) curves and electrochemical impedance spectroscopy (EIS) were

conducted on Bio-Logic system with BPC-x as cathode, Zn foil as anode and 2 M ZnSO₄ as electrolyte in a CR2032 coin cell. For EIS measurement, the applied frequency was between 10^{-2}-10^5 Hz. The long-term cycling stability test was performed on Land CA2001A system and Neware battery system. The specific capacitance (C, F g^{-1}) of carbon electrode calculated from GCD curves was obtained using the following equations:

$$C = I\Delta t/m\Delta U$$

where I (A) is the current, Δt (s) is the discharging time, m (g) is the mass of the active material and ΔU (V) is the voltage window excluding ohmic drop.

The specific capacity (C_m, mAh g^{-1}) of ZHSCs calculated from GCD curves was obtained using the following equations:

$$C_m = I\Delta t/m$$

where I (mA) is the current, Δt (h) is the discharging time, m (g) is the mass of the active material.

In-situ FTIR investigation: The electrode for *in-situ* Fourier transform infrared (FTIR) investigation was prepared by following steps. The BPC-3 active material was mixed with conductive additive (acetylene black) and binder (polytetrafluorethylene) with a weight ratio of 8:1:1 in the ethanol solvent and subsequently dried. The obtained mixtures were rolled and punched into 10 mm (diameter) round electrode sheet, and dried at 80 °C. The carbon electrode for in-situ FTIR investigation was obtained by firmly attaching the prepared film to a titanium mesh current collector. The in-situ FTIR spectroscopy was conducted using the Bruker INVENIO-R spectrometer instrument. Furthermore, cyclic voltammetry (CV) measurements were performed on the CHI760E electrochemical workstation system utilizing a two-electrode system during the *in-situ* FTIR test.

In-situ Electrochemical Raman Spectroscopy: Raman spectroscopy is an effective tool to reveal the properties of carbon-based materials and can reflect the characteristic

features including doping, defects, and stress. For a carbon material, its charging/discharging process was often accompanied by the adsorption and desorption of ions inside the porous spaces. Also, the in-situ Raman spectroscopy was employed to monitor the electrochemical behavior of electrolyte ions within the carbon material, and its Raman spectrum can be fitted by two main bands including G band at ~1590 cm^{-1} and D band at ~1340 cm^{-1}. Briefly, the *in-situ* Raman measurements were conducted during the initial two charging cycles (from 0 V to 1.8 V) and discharging cycle (from 1.8 V to 0 V) of the electrode material, while continuously recording the Raman spectra on the electrode surface. Specifically, the carbon electrode materials were prepared as described early, and Raman spectra were collected using a two-electrode system with zinc wire as the anode, BPC-3 electrode sheet as the cathode, and 2 M $ZnSO_4$ as the electrolyte.
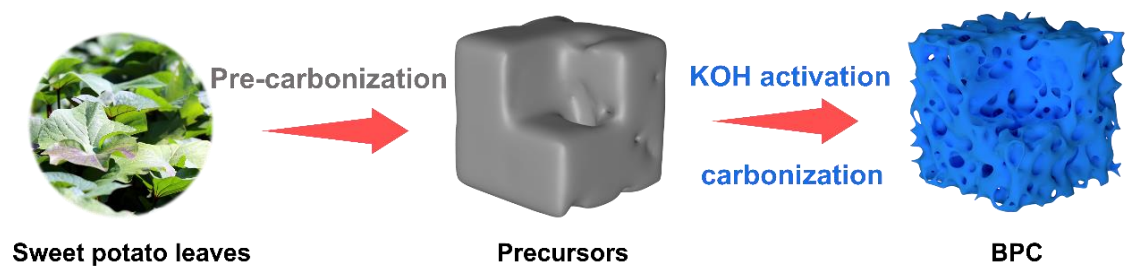
Figure S1. Schematic illustration of synthesis process for BPC-x
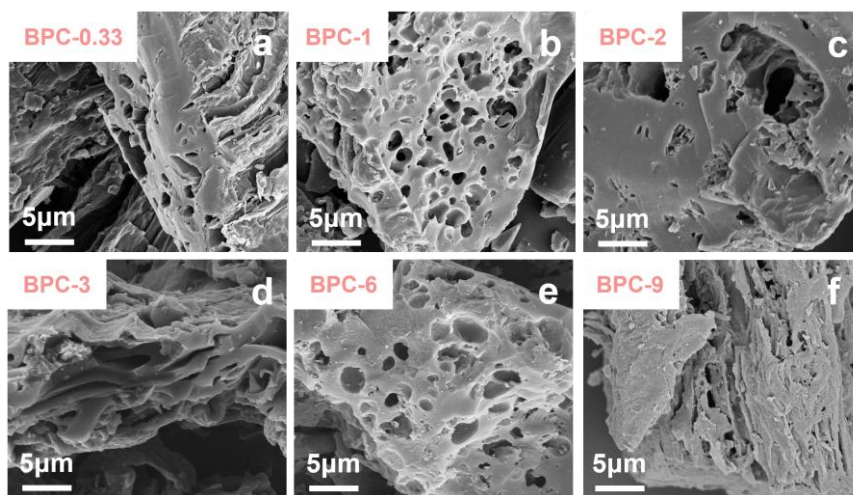
Figure S2. SEM images of (a) BPC-0.33, (b) BPC-1, (c) BPC -2, and (d) BPC -3 (e) BPC -6, (f) BPC -9.
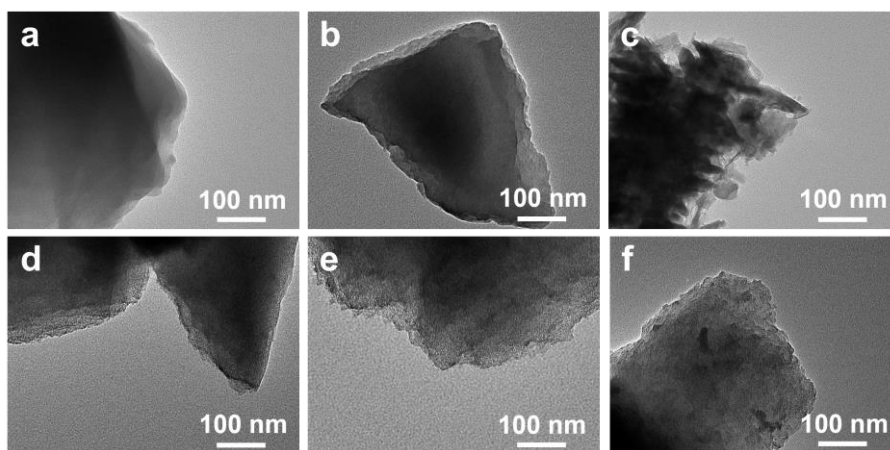
Figure S3. TEM images of (a) BPC-0.33, (b) BPC-1, (c) BPC -2, and (d) BPC -3 (e) BPC -6, (f) BPC -9.
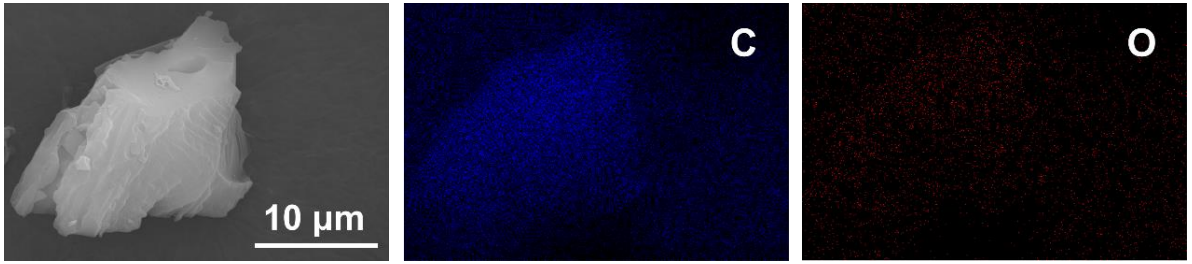
Figure S4. SEM image and corresponding mapping of BPC-3.
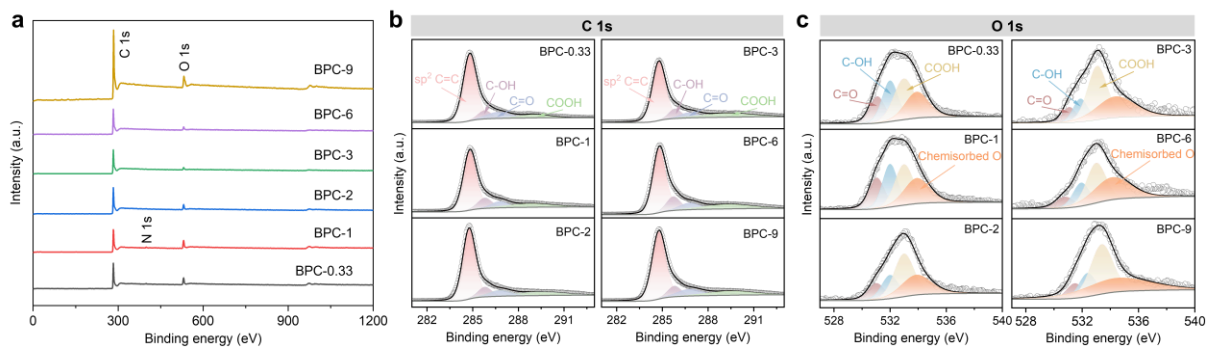
Figure S5. (a) XPS survey spectra of BPC-x, (b) C 1s, (c) O 1s XPS spectra of BPC-x.
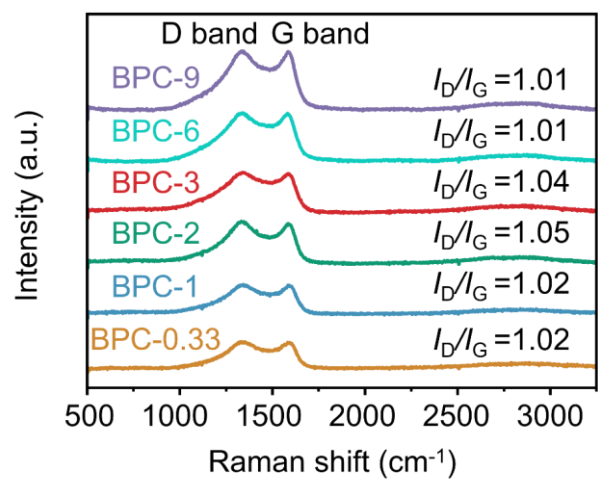
Figure S6. Raman spectra of BPC-x.
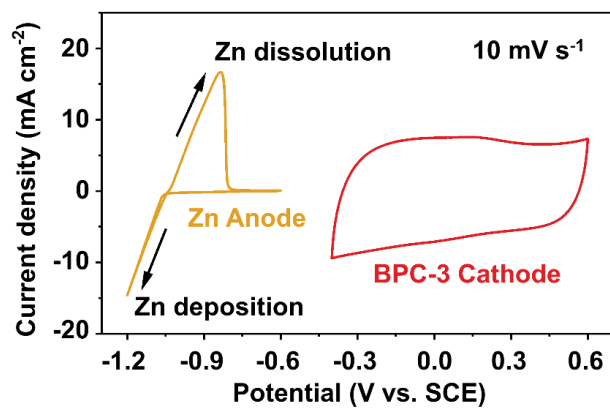
Figure S7. CV curves of Zn anode and BPC-3 cathode with 2 M ZnSO$_4$ electrolytes at 10 mV s^{-1}.
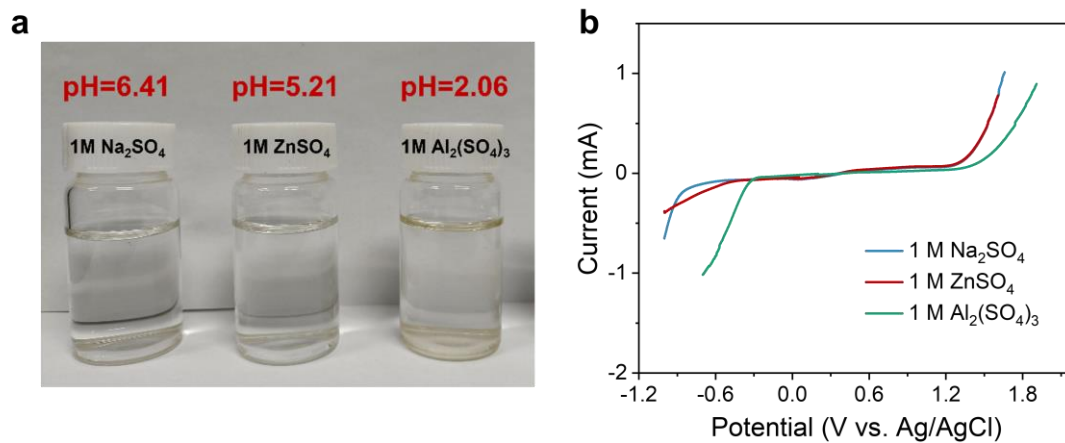
Figure S8. (a) Optical photographs of different electrolytes at room temperature and their respective pH values. (b) LSV curves of different electrolytes within a wide voltage range in a three-electrode system.
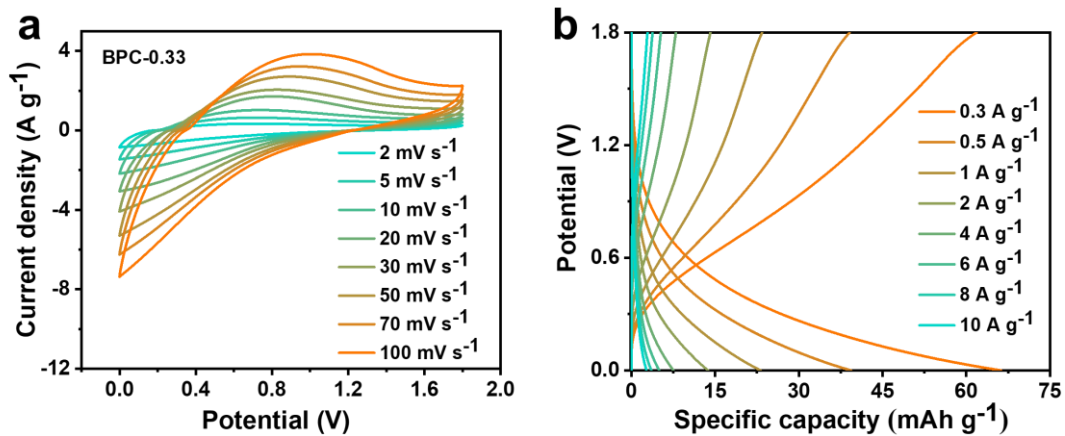
Figure S9. (a) CV curves of Zn//BPC-0.33 ZHSCs at various scan rates, (b) GCD curves of BPC-0.33 at different current densities in a two-electrode system.
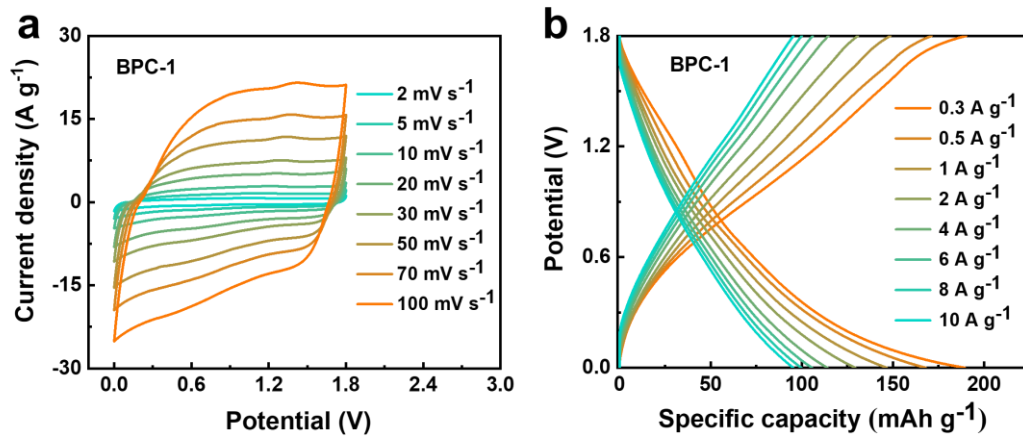
Figure S10. (a) CV curves of Zn//BPC-1 ZHSCs at various scan rates, (b) GCD curves of BPC-1 at different current densities in a two-electrode system.
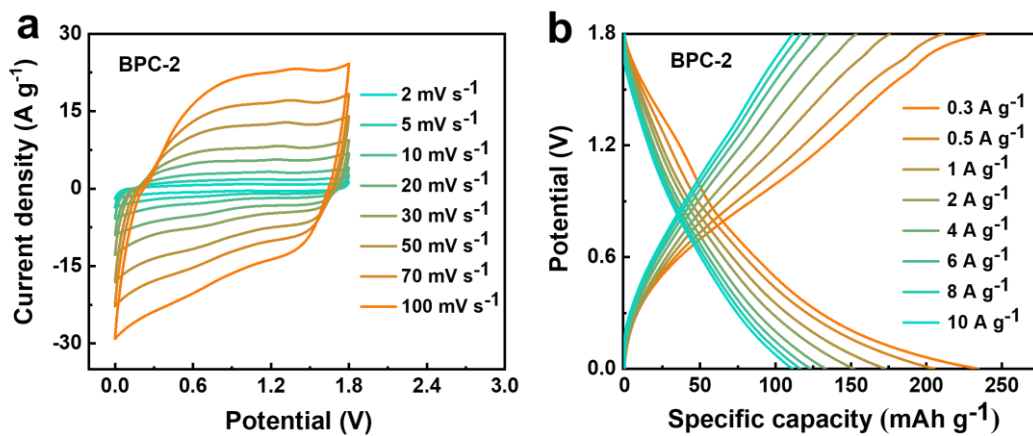
Figure S11. (a) CV curves of Zn//BPC-2 ZHSCs at various scan rates, (b) GCD curves of BPC-2 at different current densities in a two-electrode system.
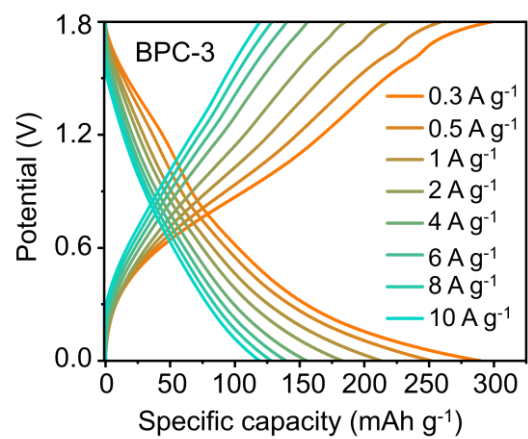
Figure S12. GCD curves of BPC-3 at different current densities in a two-electrode system.
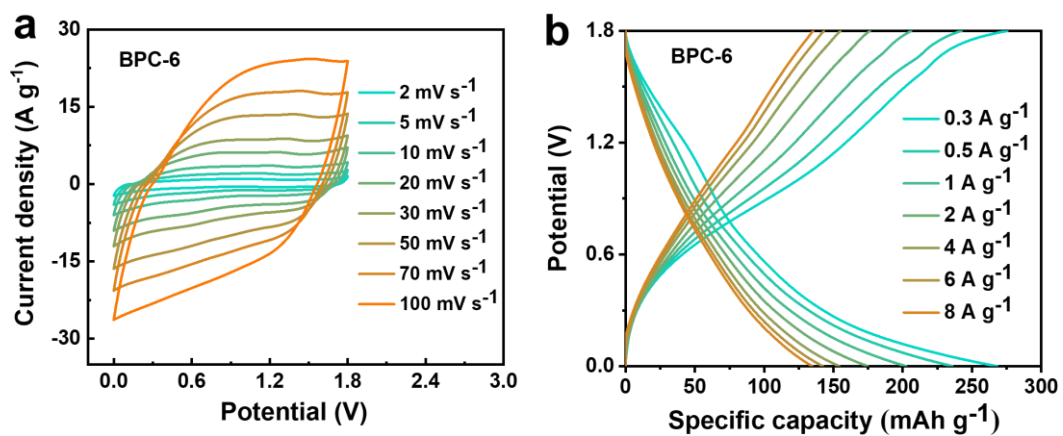
Figure S13. (a) CV curves of Zn//BPC-6 ZHSCs at various scan rates, (b) GCD curves of BPC-6 at different current densities in a two-electrode system.
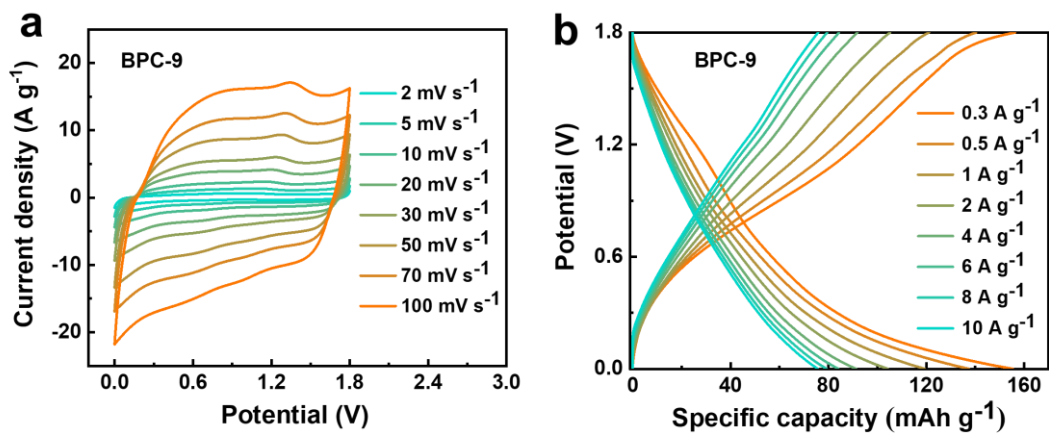
Figure S14. (a) CV curves of Zn//BPC-9 ZHSCs at various scan rates, (b) GCD curves of BPC-9 at different current densities in a two-electrode system.
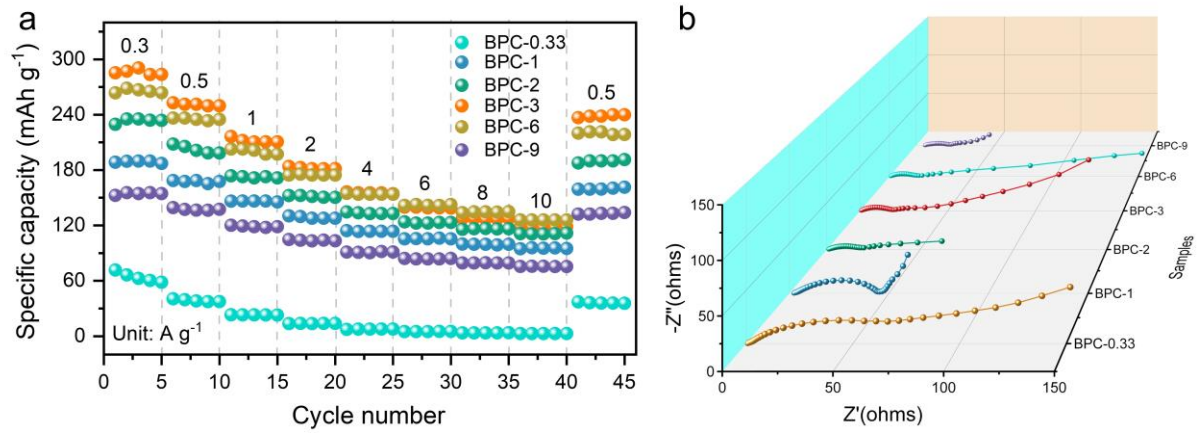
Figure S15. (a) Rate performances and (b) Nyquist impedance plots of Zn//BPC-x ZHSCs.
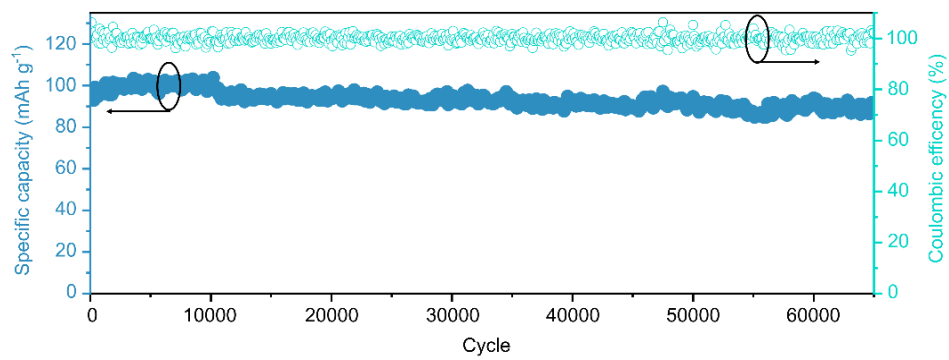
Figure S16. Long cycling stability performance of Zn//BPC-3 ZHSCs at 10 A g^{-1}.
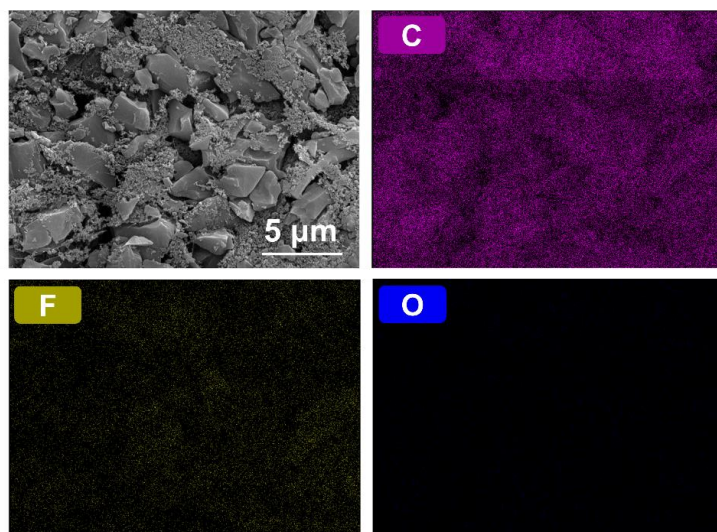
Figure S17. SEM images and corresponding elemental mapping of the BPC-3 cathode before 65,000 cycles.
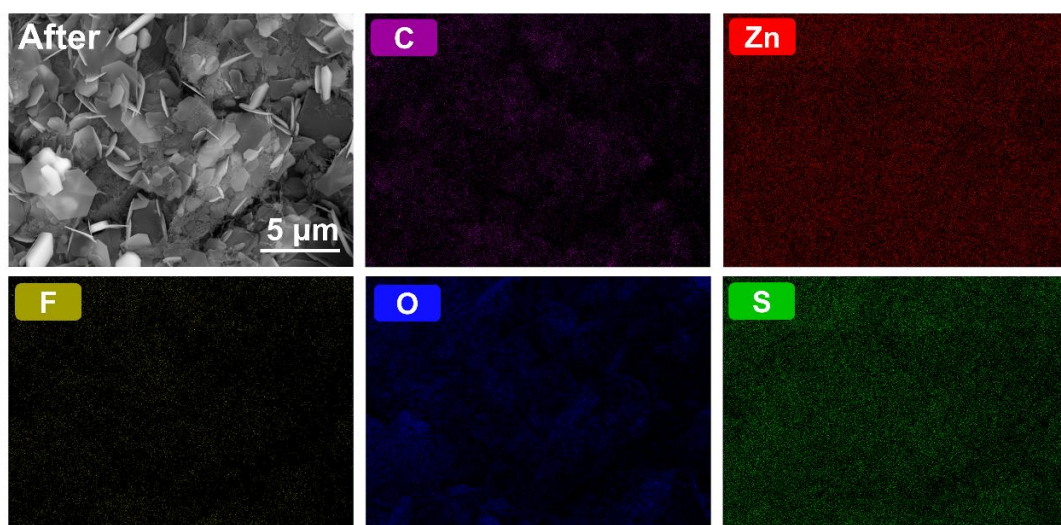
Figure S18. SEM images and corresponding elemental mapping of the BPC-3 cathode after 65,000 cycles.
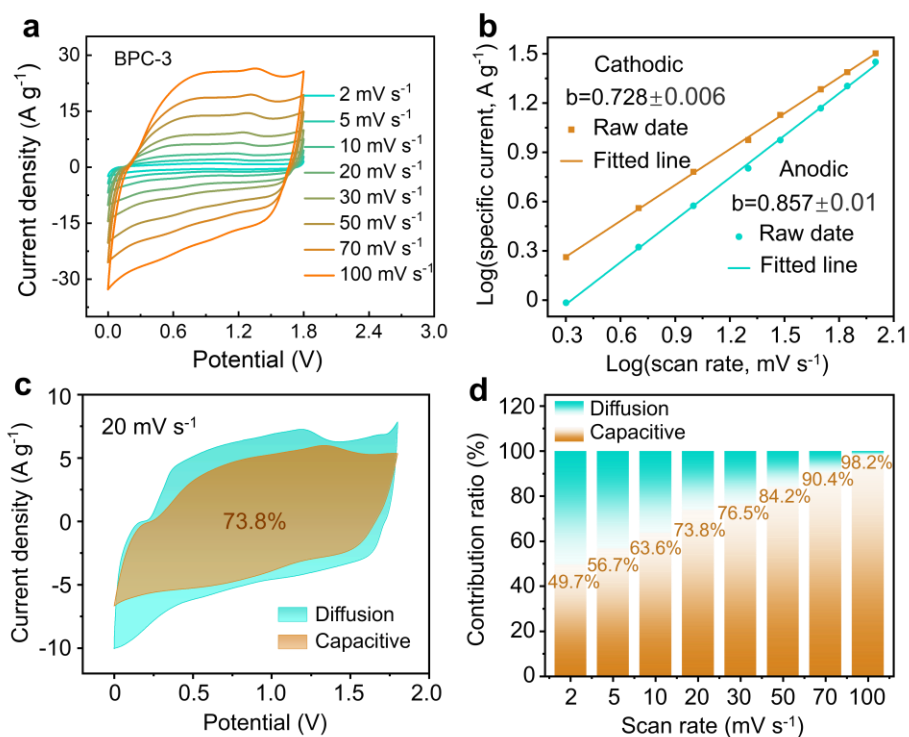
Figure S19. (a) CV curves of BPC-3 cathode at 2 to 100 mV s^{-1}. (b) The corresponding Linear relationships of log (*i*) vs. log (*v*) (peak current: *i*, scan rate: *v*). (c) The CV profiles of BPC-3 cathode with the capacitance contribution at 20 mV s^{-1}. (d) The different capacitance contributions over BPC-3 at various scan rates.
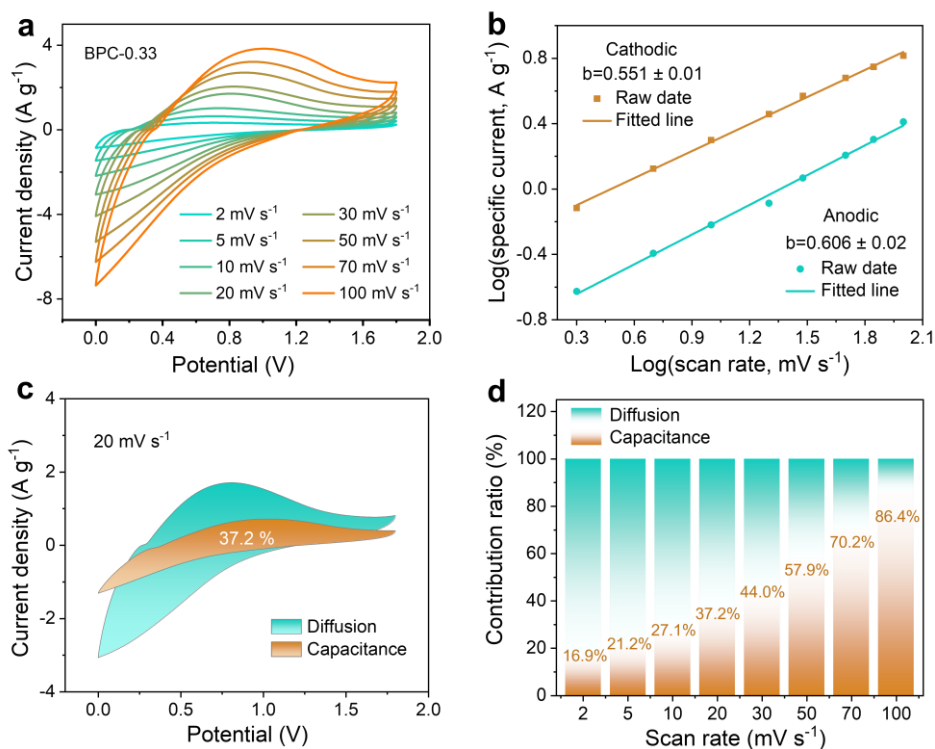
Figure S20. (a) CV curves of BPC-0.33 cathode at 2 to 100 mV s^{-1}. (b) The corresponding Linear relationships of log (i) vs. log (v) (peak current: i, scan rate: v). (c) The CV profiles of BPC-0.33 cathode with the capacitance contribution at 20 mV s^{-1}. (d) The different capacitance contributions over BPC-0.33 at various scan rates.
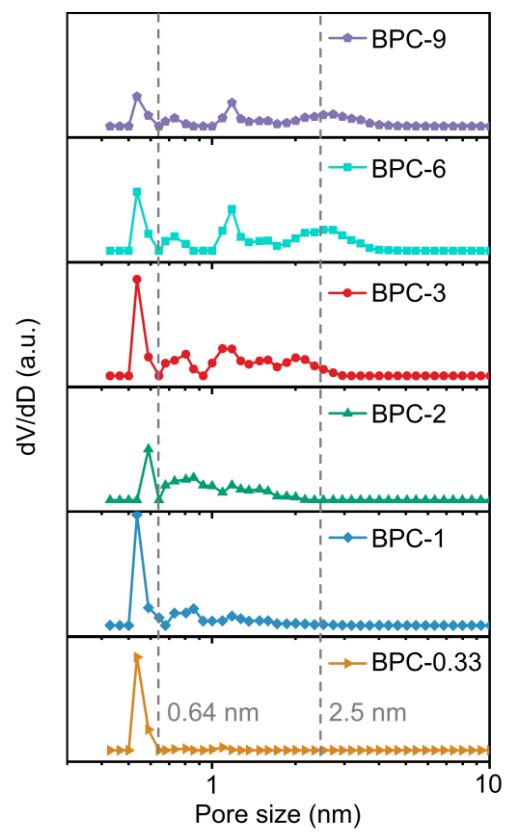
Figure S21. Pore-size distributions of BPC-x.
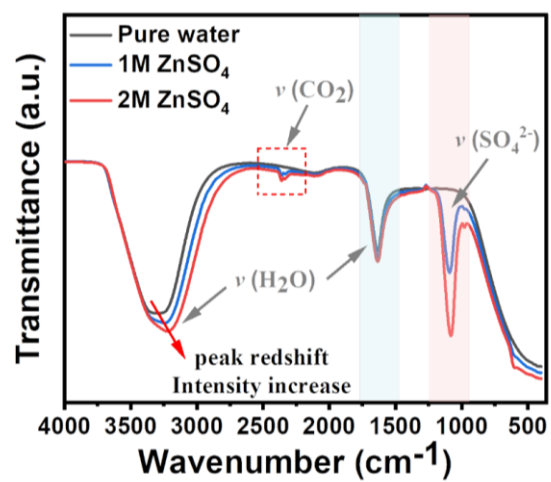
Figure S22. The FTIR spectra of different electrolytes and pure water.
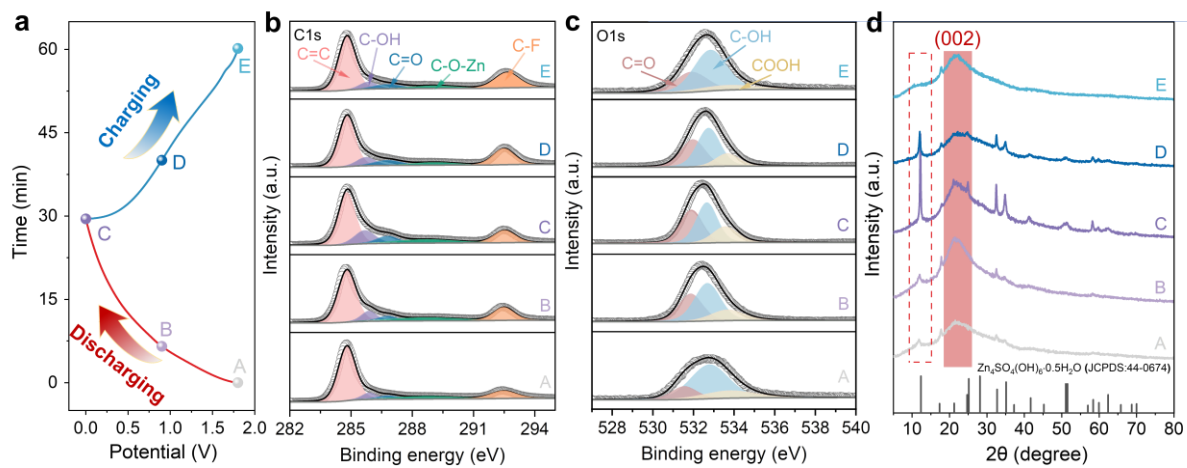
Figure S23. (a) The typical GCD curve at 0.5 A g^{-1}, (b) C 1s, and c) O 1s XPS spectra of BPC-3 cathode at different stages, (d) *Ex-situ* XRD patterns of BPC-3 cathode at different stages.
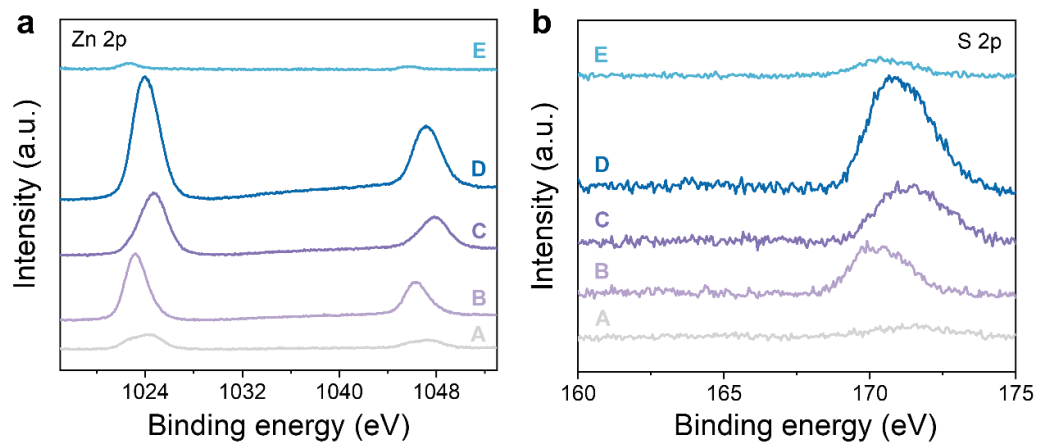
Figure S24. (a) Zn 2p and (b) S 2p XPS spectra of BPC-3 cathode at different stages.
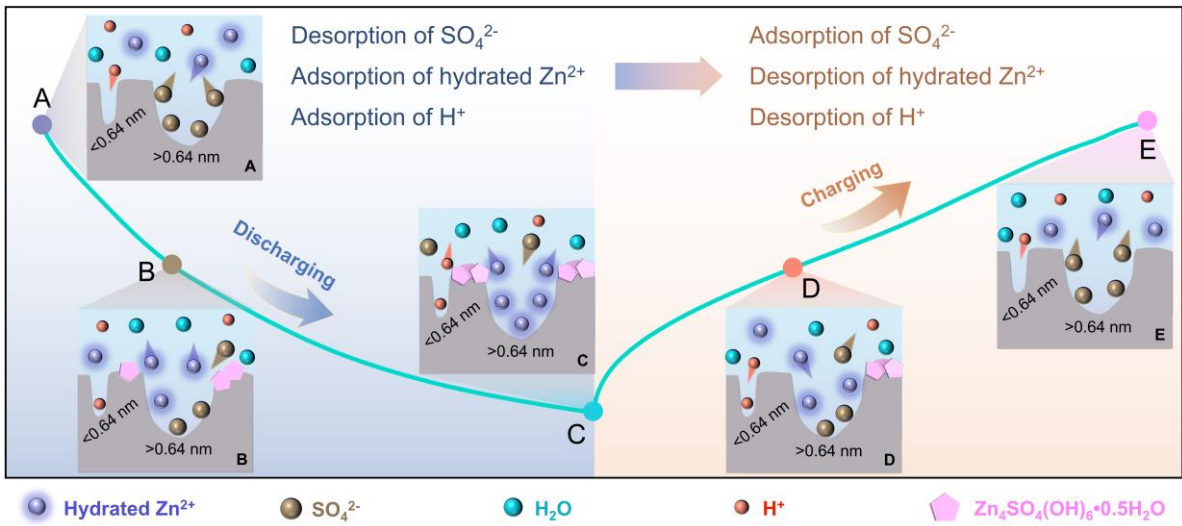
Figure S25. Schematic illustration of the charge-storage mechanism for BPC-3 in 2 M $ZnSO_4$ electrolyte.
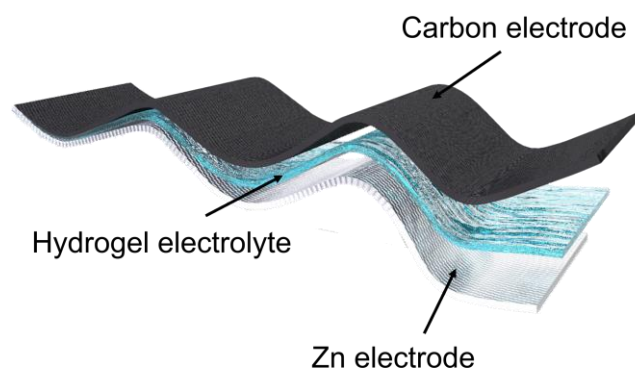
Figure S26. Structure of quasi-solid-state ZHSCs.
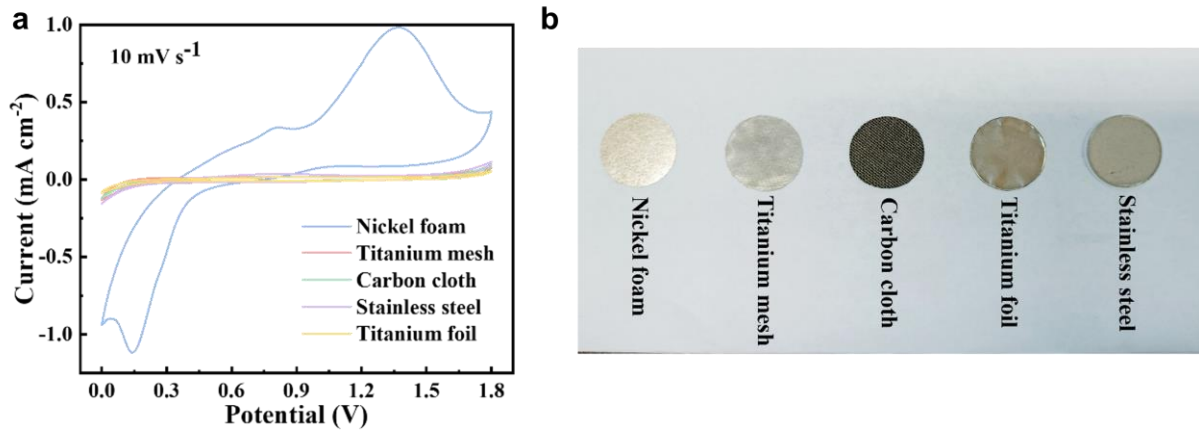
Figure S27. (a) CV curves of ZHSCs using different current collectors without active material at the scan rate of 10 mV s^{-1} in 2 M ZnSO$_4$ aqueous electrolyte. The voltage window is 0–1.8 V. (b) Digital photographs of different current collectors.

Note 1: The role of current collectors is crucial for the energy density of ZHSCs. We conducted CV tests at 10 mV s^{-1} with a 2 M ZnSO$_4$ electrolyte using five different current collectors without loaded active carbon material to explore their impact on the capacity contribution of ZHSCs. Figure S23 illustrates the individual contributions of each current collector. Among them, the foam nickel collector exhibits the highest capacity contribution, while the titanium mesh collector has minimal impact. The ultra-high specific capacitance achieved in Zn//BPC-3 ZHSCs utilizing a titanium mesh as the current collector can be mainly attributed to the contribution of BPC-3.

Table S1. Porosity parameters of BPC-x.

Sample	Specific surface area (m²/g)	Total pore volume (cm³/g)	Micropore volume (cm³/g)	Pore volume ratio		Cumulative pore volume 0.64 nm<V< 2.5 nm (cm³/g)
				Micropore	Mes/Macropore	
BPC-0.33	553	0.30	0.24	80%	20%	0.024
BPC-1	1450	0.77	0.60	78%	22%	0.346
BPC-2	1994	1.05	0.85	81%	19%	0.616
BPC-3	3064	1.62	1.10	68%	32%	1.145
BPC-6	3846	2.16	0.79	37%	63%	1.095
BPC-9	2137	1.26	0.40	32%	68%	0.559

Table S2. Electrochemical performance comparison of Zn//BPC-3 ZHSCs with previously reported advanced carbon-material-based ZHSCs.

Cathode	Loading (mg cm^{-2})	Electrolyte	surface area (m^2 g^{-1})	average pore width (nm)	Rate performance (@ A g^{-1})	Ref.
BPC-3	**2.1**	**2M ZnSO$_4$**	**3064**	**0.64-3**	**290 mAh g^{-1} @ 0.3** **580 F·g^{-1}@0.3**	**This work**
Zn$_1$Cux–MOF@C	~1.0	2 M ZnSO$_4$@PAM	910	18	134 mAh g^{-1} @ 0.5	[1]
AC-SA	1.9~10	2M ZnSO$_4$	2066	1.2–2	436 F·g^{-1}@0.02 166.3 mAh·g^{-1}@0.2	[2]
rGO	1.2~1.5	1 m ZnSO$_4$	N.A	N.A	245 F g^{-1} at 0.5	[3]
ANHP-2	1.0	2M ZnSO$_4$	3553	1.2–2	199.1mAh g^{-1}@0.5	[4]
APC	0.5~0.7	1M ZnCl$_2$	1566	0.5-1 & 4	255.2 mAh g^{-1}@0.3	[5]
NHG	1.0	2 m ZnCl$_2$	325	0.72–0.81	235.4 F cm^{-3} @0.1	[6]
ACF	10.3	2M ZnSO$_4$	2454	0.6-2	246 mAh g^{-1}@0.2	[7]
ZDC	2–15	2M ZnSO$_4$	1347	0-2	310 F g^{-1} @0.5	[8]
L-CNSs	2.5-3.0	1 m ZnSO$_4$	587	0.5 & 0.65	233.4 F g^{-1} @ 0.1	[9]
AC	N.A	2 m ZnSO$_4$ +0.1 m MgSO$_4$	1535	1.6-2.4	154 mA h g^{-1} @1	[10]
AC	0.8	2 m ZnCl$_2$	2053	1.5-2.5	481.4 F·g^{-1}@0.5 229.4 F·g^{-1}@1	[11]
HPCF	N.A	2 m ZnSO$_4$	2000	0.68-2	141mAh g^{-1}@0.1	[12]
PN-CHoNS	1.1-1.5	2 M ZnSO$_4$	30	N.A	164.4mAh g^{-1}@0.2	[13]
OCC	0.3	saturated Zn(CF$_3$SO$_3$)$_2$	1733	1.5 & 3.5	225 mAh g^{-1} @0.1	[14]
BGC	1.0	3 M Zn(CF$_3$SO$_3$)$_2$	3657	1.5-4	257 mAh g^{-1} @0.5	[15]
HPAC	0.6	3 M Zn(CF$_3$SO$_3$)$_2$	3525	1.2 & 2-4	231 mAh g^{-1} @0.5	[16]
NTC	1-1.5	1 m ZnSO$_4$	844	1	341.2 F·g^{-1}@0.1	[17]
PC	1.75	3 M Zn(ClO$_4$)$_2$	1095	1.5	340.7 F g^{-1}@0.1 179.8 mAh g^{-1} @0.1	[18]
rGO	1.75-3.25	1 m ZnSO$_4$	198	N.A	277 F g^{-1} @1 mV/s	[19]

MCHSs	1-20	2M $ZnSO_4$	1275	1.2 & 10.7	174.7 mAh g^{-1}@0.1	[20]
PSC	2.0	1M $Zn(CF_3SO_3)_2$	948	0.8 & 1.1	413.3 F g^{-1}@0.2	[21]
Sn-Ti$_2$CTX/C	N.A	21M LiTFSI + 1M $Zn(OTf)_2$	N.A	N.A	138 mAh g^{-1}@0.1	[22]
DFs	N.A	1.0 m $ZnSO_4$	N.A	N.A	246.1F g^{-1}@0.2	[23]
HPC	1.5-2.0	2.0 M $ZnSO_4$	197	1.2 & 2.5	138.5 mA h g^{-1}@0.5	[24]
AC	N.A	2M $ZnSO_4$	2201	N.A	468 F·g^{-1}@0.5	[25]
aMEGO	N.A	3 m $Zn(CF_3SO_3)_2$	2957	1, 2, & 4	213 F·g^{-1}@0.1	[26]
AC	6.0	2M $ZnSO_4$	1990	0.5, 0.8 & 1.2	132 mAh·g^{-1}@0.1	[27]
LDC	2.0	1 M $ZnSO_4$	597	0.43 & 3.76	127.7mAh·g^{-1}@0.5	[28]
N-HPC	1.0	2M $ZnSO_4$	879	0.5, 1.2 & 1.8	136.8 mAh·g^{-1}@0.1	[29]
AC	N.A	1 M $Zn(CF_3SO_3)_2$	3384	2.5	170 F g^{-1} @0.1	[30]
AC	0.7-0.8	2 M $ZnSO_4$	1923	1.2-2.7	121 mAh g^{-1}@0.1	[31]

References

[1] H. Zhang, H. Wang, Z. Pan, Z. Wu, Y. Deng, J. Xie, J. Wang, X. Han and W. Hu. *Adv. Mater.,* **2022**, 34, 2206277.

[2] Z. Xu, R. Ma and X. Wang. *Energy Storage Mater.,* **2022**, 46, 233-242.

[3] H. Xu, W. He, Z. Li, J. Chi, J. Jiang, K. Huang, S. Li, G. Sun, H. Dou and X. Zhang. *Adv. Funct. Mater.,* **2022**, 32, 2111131.

[4] L. Wang, M. Peng, J. Chen, T. Hu, K. Yuan and Y. Chen. *Adv. Mater.,* **2022**, 34, 2203744.

[5] X. Shi, J. Xie, F. Yang, F. Wang, D. Zheng, X. Cao, Y. Yu, Q. Liu and X. Lu. *Angew. Chem., Int. Ed.,* **2022**, 61, e202214773.

[6] J. Luo, L. Xu, H. Liu, Y. Wang, Q. Wang, Y. Shao, M. Wang, D. Yang, S. Li, L. Zhang, Z. Xia, T. Cheng and Y. Shao. *Adv. Funct. Mater.,* **2022**, 32, 2112151.

[7] X. Li, Y. Li, X. Zhao, F. Kang and L. Dong. *Energy Storage Mater.,* **2022**, 53, 505-513.

[8] C. Leng, Y. V. Fedoseeva, Z. Zhao, B. Yan, A. V. Okotrub, X. Wang, J. Fan and J. Qiu. *J. Power Sources,* **2022**, 536, 231484.

[9] W. Jian, W. Zhang, X. Wei, B. Wu, W. Liang, Y. Wu, J. Yin, K. Lu, Y. Chen, H. N. Alshareef and X. Qiu. *Adv. Funct. Mater.,* **2022**, 32, 2209914.

[10] P. Wang, X. Xie, Z. Xing, X. Chen, G. Fang, B. Lu, J. Zhou, S. Liang and H. J. Fan. *Adv. Energy Mater.,* **2021**, 11, 2101158.

[11] C. Wang, Z. Pei, Q. Meng, C. Zhang, X. Sui, Z. Yuan, S. Wang and Y. Chen. *Angew. Chem., Int. Ed.,* **2021**, 60, 990-997.

[12] Y. Li, W. Yang, W. Yang, Z. Wang, J. Rong, G. Wang, C. Xu, F. Kang and L. Dong. *Nano-Micro Lett.,* **2021**, 13, 1-16.

[13] J. Li, J. Zhang, L. Yu, J. Gao, X. He, H. Liu, Y. Guo and G. Zhang. *Energy Storage Mater.,* **2021**, 42, 705-714.

[14] C. C. Hou, Y. Wang, L. Zou, M. Wang, H. Liu, Z. Liu, H. F. Wang, C. Li and Q. Xu. *Adv. Mater.,* **2021**, 33, 2101698.

[15] W. Fan, J. Ding, J. Ding, Y. Zheng, W. Song, J. Lin, C. Xiao, C. Zhong, H. Wang and W. Hu. *Nano-Micro Lett.,* **2021**, 13, 1-18.

[16] Z. Zhou, X. Zhou, M. Zhang, S. Mu, Q. Liu and Y. Tang. *Small,* **2020**, 16, 2003174.

[17] R. Yuksel, O. Buyukcakir, P. K. Panda, S. H. Lee, Y. Jiang, D. Singh, S. Hansen, R. Adelung, Y. K. Mishra, R. Ahuja and R. S. Ruoff. *Adv. Funct. Mater.,* **2020**, 30, 1909725.

[18] J. Yin, W. Zhang, W. Wang, N. A. Alhebshi, N. Salah and H. N. Alshareef. *Adv. Energy Mater.,* **2020**, 10, 2001705.

[19] Y. Shao, Z. Sun, Z. Tian, S. Li, G. Wu, M. Wang, X. Tong, F. Shen, Z. Xia, V. Tung, J. Sun and Y. Shao. *Adv. Funct. Mater.,* **2020**, 31, 2007843.

[20] P. Liu, W. Liu, Y. Huang, P. Li, J. Yan and K. Liu. *Energy Storage Mater.,* **2020**, 25, 858-865.

[21] Z. Li, D. Chen, Y. An, C. Chen, L. Wu, Z. Chen, Y. Sun and X. Zhang. *Energy Storage Mater.,* **2020**, 28, 307-314.

[22] X. Li, M. Li, Q. Yang, D. Wang, L. Ma, G. Liang, Z. Huang, B. Dong, Q. Huang and C. Zhi. *Adv. Energy Mater.,* **2020**, 10, 2001394.

[23] Z. Jian, N. Yang, M. Vogel, S. Leith, A. Schulte, H. Schönherr, T. Jiao, W. Zhang, J. Müller, B. Butz and X. Jiang. *Adv. Energy Mater.,* **2020**, 10, 2002202.

[24] X. Deng, J. Li, Z. Shan, J. Sha, L. Ma and N. Zhao. *J. Mater. Chem. A,* **2020**, 8, 11617-11625.

[25] G. H. An, J. Hong, S. Pak, Y. Cho, S. Lee, B. Hou and S. Cha. *Adv. Energy Mater.,* **2019**, 10, 1902981.

[26] S. Wu, Y. Chen, T. Jiao, J. Zhou, J. Cheng, B. Liu, S. Yang, K. Zhang and W. Zhang. *Adv. Energy Mater.,* **2019**, 9, 1902915.

[27] Z. Wang, J. Huang, Z. Guo, X. Dong, Y. Liu, Y. Wang and Y. Xia. *Joule,* **2019**, 3, 1289-1300.

[28] Y. Lu, Z. Li, Z. Bai, H. Mi, C. Ji, H. Pang, C. Yu and J. Qiu. *Nano Energy*, **2019**, 66, 104132.

[29] P. Liu, Y. Gao, Y. Tan, W. Liu, Y. Huang, J. Yan and K. Liu. *Nano Res.,* **2019**, 12, 2835-2841.

[30] H. Wang, M. Wang and Y. Tang. *Energy Storage Mater.,* **2018**, 13, 1-7.

[31] L. Dong, X. Ma, Y. Li, L. Zhao, W. Liu, J. Cheng, C. Xu, B. Li, Q.-H. Yang and F. Kang. *Energy Storage Mater.,* **2018** 13, 96-102.